International Journal of Infrared and Millimeter Waves, Vol. 9, No. 12, 1988

EFFECT OF IMPACT IONIZATION ON THE SATURATION OF 1s− 2p$_+$ SHALLOW DONOR TRANSITION IN n-GaAs

M. Weispfenning, F. Zach, and W. Prettl

Institut für Angewandte Physik
Universität Regensburg
8400 Regensburg, W. Germany

Received September 13, 1988

The magneto-photoconductivity due to 1s-2p$_+$ optical transitions of shallow donors in n-GaAs has been investigated as a function of intensity for several bias voltages at low temperatures between 2 K and 4.2 K. At low intensities a superlinear increase of the photoconductive signal with rising intensity has been observed which gets more pronounced at higher bias voltages and lower temperatures. The power broadening of the linewidth was found to be distinctly different from the behaviour expected for a two-level system. By a detailed analysis in terms of a nonlinear generation-recombination model it is shown that these effects may be attributed to impact ionization of the optically excited 2p$_+$ states.

Keyword: shallow donors, nonlinear magneto-photoconductivity, saturation, impact ionization.

Introduction

The kinetics of electrons bound to shallow impurities at low temperatures in high purity semiconductors may be studied by saturation spectroscopy in the far-infrared (FIR) spectral range. Several investigations involving resonant impurity transitions and cyclotron resonance were carried out applying FIR molecular lasers pumped by TEA-CO_2 lasers [1-3], quasi-cw lasers pumped by electrically pulsed low pressure CO_2 lasers [4-7], and recently the UCSB free-electron laser [8,9]. The most detailed measurements were performed on the 1s-2p$_+$ shallow donor transitions of n-GaAs epitaxial layers in an external magnetic field. As a function of the laser intensity incident on the sample the absorption coefficient and the photoconductive

0195-9271/88/1200-1153$06.00/0

signal due to 1s-$2p_+$ optical transitions have been measured for various magnetic field strengths. The experimental results were analyzed in terms of appropriate rate equation models assuming that a fraction of electrons excited to the $2p_+$ donor state are transferred to the conduction band by thermal action in the sense of the photothermal effect which was first proposed by Kogan et al. [10]. Measurements obtained by cw-lasers in the power range up to typically 100 mW/cm^2 have been described by $\alpha_o \propto (1 + \frac{I}{I_S})^{-1}$ and $\Delta V_o \propto I(1 + \frac{I}{I_S})^{-1}$ where α_o and ΔV_o are the absorption coefficient and the photosignal, respectively, both at line center. These simple relations are expected for the absorption of a two-level system and a simple photoionization process, respectively [11]. Very low saturation intensities I_S were observed leading to effective time constants τ_{eff} in the order of several 10 ns, where τ_{eff} is the average time optically excited electrons need to return to the donor ground states.

Higher power levels with pulse durations longer than τ_{eff}, which are necessary to obtain steady state conditions during irradiation, are now available by the UCSB free-electron laser. First measurements showed that the photoconductive signal significantly deviates from the above relation for high intensities. This was attributed to direct photoionization processes in addition to the resonant photothermal ionization accross the $2p_+$ state. An analysis of the experimental results yielded in addition to the effective time constant τ_{eff} the ionization probability of the $2p_+$ state, the nonradiative $2p_+$-1s transition time and the recombination time of free electrons [8,9].

In the present investigation we show that even for low intensities the description of photoconductivity saturation given above, $\Delta V_o \propto I(1+\frac{I}{I_S})^{-1}$, does not satisfactorily describe the experimental observations. For very low intensities the photosignal was found to increase superlinearly with rising intensity. The observed phenomena are qualitatively similar to that of the cyclotron resonance induced photoconductivity [7]. The magnitude of the effect, however, is much smaller than in the latter case. The superlinear intensity dependence is observed down to the lowest practically applicable bias voltages and gets more pronounced for lower temperatures. From these observations we conclude that besides thermal ionization of the optically populated $2p_+$ level impact ionization of the excited state contributes to the photoconductive signal in a non-negligible extent. Impact ionization occurs at very low or even vanishing electric bias fields due to the optically produced nonthermal electron distribution.

A further problem of the saturation of shallow impurity resonances is the intensity dependence of the line width which has not yet

been analyzed in detail. The saturation relation $\Delta V_o \propto I/(1+\frac{I}{I_S})^{-1}$ leads to the well-known power broadening $\Delta\omega \propto (1+\frac{I}{I_S})^{1/2}$ if the non-saturated optical absorption cross section has a Lorentzian shaped dependence on frequency. Our measurements show that $\Delta\omega \propto (1+\frac{I}{I_S})^{1/2}$ is not realized over a substantially large intensity range. For low intensities the excited state impact ionization leads to a reduction of the power broadening in comparison to the above relation. At higher power levels $\Delta\omega$ follows this relation more closely, however saturation intensities evaluated from power broadening are typically smaller than those obtained from the peak photoconductive signal [9].

Experimental

(a) Technique

Several high purity n-GaAs epitaxial layers prepared by liquid phase epitaxy on semiinsulating substrates were investigated. Wedged pieces of polished semiinsulating GaAs were glued by parafine oil on the substrate face of the samples. Measurements of the photoconductivity spectrum using an FIR Fourier transform spectrometer showed that optical interferences in the samples were completely suppressed by this method. Thus the intensity in the samples could be determined by taking into account the reflexion losses at front surface of the epitaxial layers. The samples were mounted in the center of a superconducting magnet and immersed in liquid helium. The measurements were carried out in Faraday configuration with the electric bias field perpendicular to the magnetic field. An electrically pulsed Edinburgh Instruments CO_2 laser was used to pump a FIR molecular laser at seven different wave-lengths between $\lambda = 118\mu m$ and 202 μm. By tuning the pressure in the FIR laser for all wavelengths single line emission could be achieved. The pulse duration was 100 μs, which is longer than any expected relaxation time ensuring steady state conditions during irradiation. The laser light was collimated by a spherical mirror with the focus slightly behind the sample to obtain homogeneous irradiation. The intensity in front of the samples was measured by a calibrated pyroelectric detector. For all laser lines the radiation was linearly polarized. As $1s\text{-}2p_+$ transitions are excited by right or left circular polarized light depending on the orientation of the magnetic field strength, the effective intensity is only one half of the total intensity irradiated on the sample. Reversing the magnetic field did not change the strength of the photoconductive signal proving the linear polarized state of the laser radiation.

The photoconductive signal was recorded by standard boxcar technique applying a load resistor circuit. In all cases the load resistor was chosen to be much smaller than the sample resistance. Therefore, and because the mobility of n-GaAs at low temperatures

is not appreciably affected by optical excitation of shallow donors [12,8,9], it follows that the relative voltage change $\Delta V/V$ across the sample is proportional to the optically generated free carrier concentration Δn.

(b) Results

The effects being reported here were found in all samples for all wavelengths and got more pronounced with rising magnetic field strength. Therefore we present measurements obtained at λ = 118 μm corresponding to a resonance magnetic field B_o = 3.6 T where the anomalies are most clearly observed. In this case, the shallow donor $2p_+$ level is about 3 meV above the band edge. In Fig. 1 the relative photoconductive signal $\Delta V/V$ normalized by the intensity I is plotted as a function of the magnetic field B in the vicinity of the resonance for three different intensities. The $1s\text{-}2p_+$ transition is observed as a practically Lorentzian shaped line on a continuous background photoconductivity due to non-resonant photoionization of shallow donors. The measurements demonstrate the saturation and power broadening of the $1s\text{-}2p_+$ transition. In addition to this line a weak structure is observed below the $1s\text{-}2p_+$ resonance field being caused by optical transitions from the 1s level to the $(Nm\lambda) = (110)$ metastable donor state, where $(Nm\lambda)$ are high field hydrogen atom quantum numbers [13]. The resonant photoconductive signal has been evaluated by substracting the continuous background photoconductivity which was determined by averaging the magnetic field dependence of the background on both sides

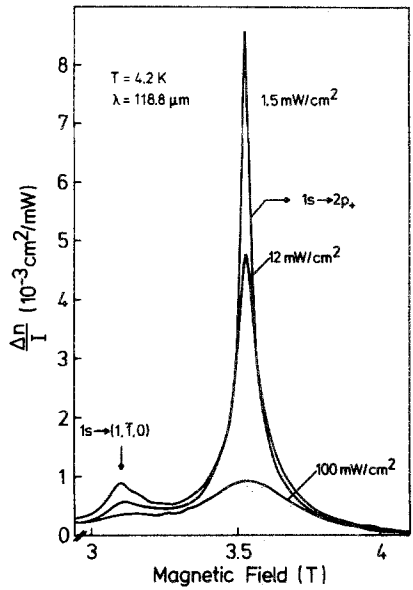

Fig. 1 — Relative intensity normalized photoconductive signal $\Delta V/(VI)$ in the vicinity of the $1s\text{-}2p_+$ resonance for three different intensities I at λ = 118 μm. Sample data: $N_D - N_A = 1.3 \cdot 10^{-14}$ cm^3, mobility at 77 K μ = 89490, thickness of the epitaxial layer d = 16 μm.

of the 1s-$2p_+$ line. The background photosignal was found to depend linearly on the intensity without saturation in the range of the present investigation. As shown previously, about two orders of magnitude larger intensities than available from cw-molecular lasers are required to saturate nonresonant photoionization of shallow donors in n- GaAs [8]. In Fig. 2 the peak resonant photosignal is shown as a function of intensity obtained at temperatures of 4.2 K (Fig. 2a) and 2 K (Fig. 2b). In both cases measurements are plotted for

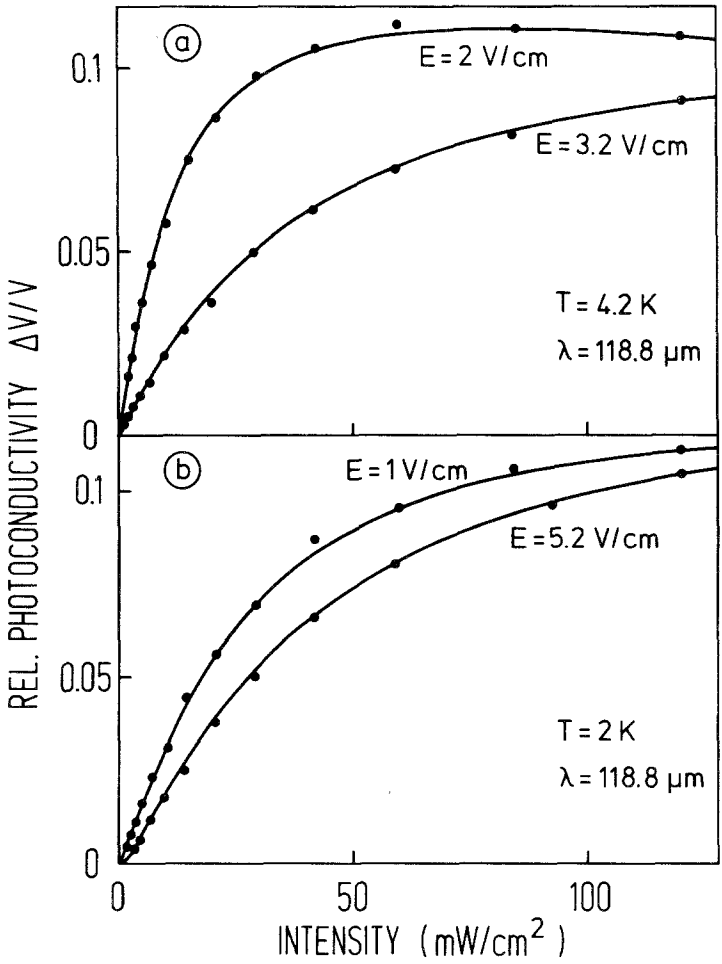

Fig. 2 — Relative photoconductive signal $\Delta V/V \propto \Delta n$ for two electric bias fields E at (a) 4.2 K and (b) 2 K. Dots are measured values, full lines are calculated curves.

two different electric bias fields E. At high intensities the photoconductive signal approaches saturation and eventually assumes a maximum and decreases with rising intensity (4.2 K, E =2 V/cm). At much higher intensitiy levels the resonant line vanishes totally due to depletion of the 1s ground state by nonresonant photoionization of the donors [9]. At low intensities the photosignal seems to be a linear function of intensity, a closer inspection of the measurements shows however that the signal actually grows superlinearly at very low intensities. The superlinear increase of the resonant photosignal is most clearly demonstrated by plotting the inverse of the intensity normalized relative signal, $S = \frac{I}{(\Delta V/V)}$, as shown in Fig. 3a and b.

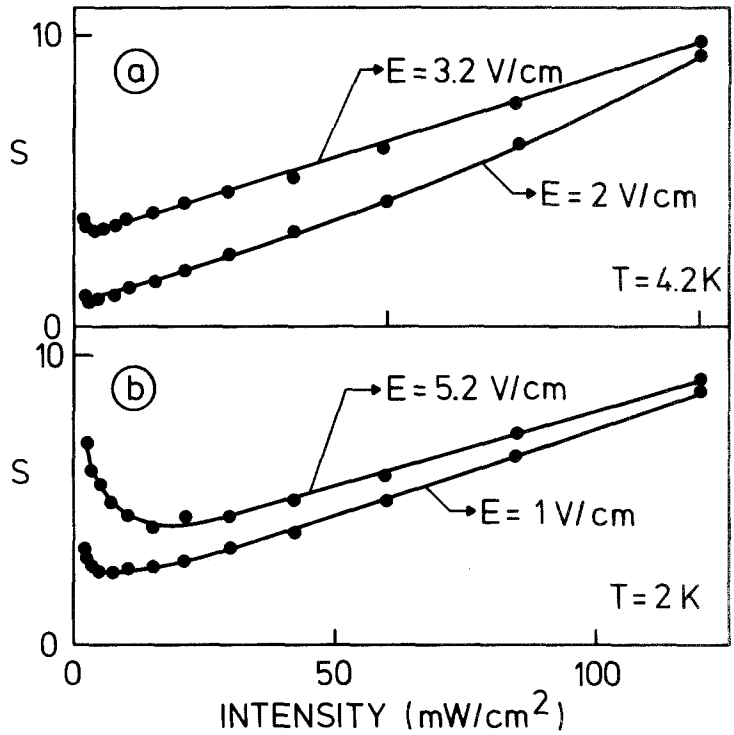

Fig. 3 — Inverse intensity normalized relative photosignal $S = \left(\frac{\Delta V/V}{I}\right)^{-1}$ as function of intensity for two bias fields E at (a) 4.2 K and (b) 2 K. Dots are measured, full lines are calculated.

From the simple saturation relation $\Delta V \propto I(1 + \frac{I}{I_S})^{-1}$ we expect a linear dependence, $S \propto 1 + \frac{I}{I_S}$ which, extrapolated to negative intensities, intersects the abszissa at $I = -I_S$. The measurements show that the inverse normalized signal is definitely no linear function of I. With decreasing intensity it rises again and assumes a relative maximum at $I = 0$ which is a consequence of the superlinear increase of the photosignal at low intensities. This effect gets more pronounced when the bias voltage is increased or the temperature is lowered as demonstrated in Fig. 3.

Fig. 4 shows the square of the linewidth as a function of intensity obtained from two typical measurements at 4.2 K and 2 K. Only the low intensity range up to 25 mW cm^{-2} is plotted in order to demonstrate the observed anomaly most clearly. Again the expected linear relation $\Delta\omega^2 \propto 1 + \frac{I}{I_S}$ is not realized. At 4.2 K with rising intensity $\Delta\omega^2$ first decreases, assumes a minimum, and then continuously increases. On the other hand at 2 K the linewidth, and thus the line itself, seems to vanish at a finite intensity indicating a thresholdlike onset of the resonant photoconductivity. The latter behaviour is qualitatively analogous to cyclotron resonance induced photoconductivity with the only difference that the intensity threshold of the photoconductivity onset is much smaller than in the case of cyclotron resonance [7].

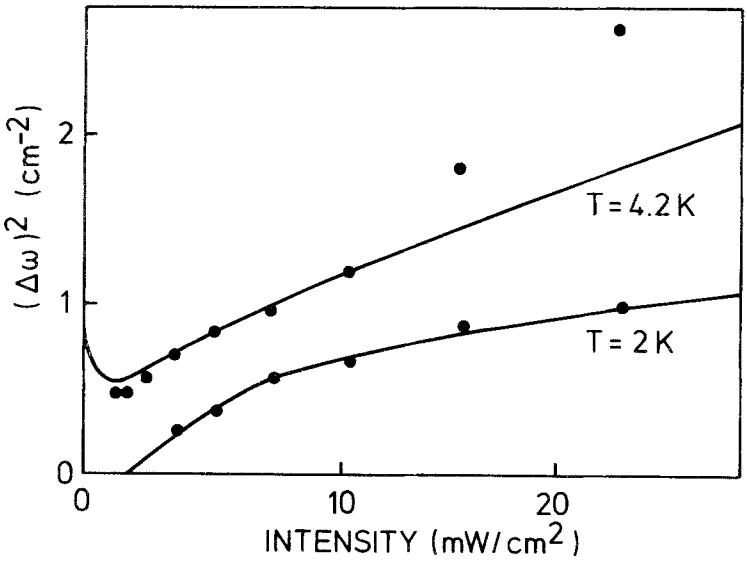

Fig. 4 — Squared linewidth $\Delta\omega^2$ as function of intensity for 4.2 K ($E = 2$ V/cm) and 2 K ($E = 1$ V/cm). Dots are measured, full lines are calculated.

At high intensities $\Delta\omega^2$ approaches a linear dependence on I. If we ignore the low intensity data however and approximate both $\Delta\omega^2$ and S a linear functions of intensity we find different apparent saturation intensities from both quantities in contradiction to the simple saturation theory. In particular saturation intensities derived from $\Delta\omega^2$ are systematically smaller than those obtained from the peak signal [9]. This observation cannot be explained by assuming an inhomogeneously broadened line. In this case the power broadening must be weaker and a larger apparent saturation intensity for $\Delta\omega$ than that of S is expected. Hence we may assume that the 1s-$2p_+$ line is homogeneously broadened however the saturation behaviour and the power broadening are effected by impact ionization of optically excited shallow donors.

Theory

a) Rate equation model

In order to describe the experimental results we extend the rate equation model used previously in [8] by the excited state impact ionization process. Fig. 5 shows a schematic energy level diagram including the 1s donor ground state, the $2p_+$ excited state and the N = 0 Landau band continuum shown by the shaded area. The generation-recombination processes being of importance at low temperatures are indicated by arrows. Electrons are excited from the donor ground state either into the $2p_+$ level or directly into the conduction band with transition probabilities $\sigma_r F$ and $\sigma_c F$, respectively. Here $F = I/\hbar\omega$ is the photon flux density with I the intensity of left or right circular polarized light and σ_r and σ_c are the corresponding optical absorption cross sections. Electrons in the $2p_+$ state are transferred into the conduction band by thermal action or by impact ionization. These processes are introduced by the kinetic coefficients X_2^S and X_2, respectively. On the other hand electrons may remain stuck in the $2p_+$ state and relax to the ground state by stimulated emission, $\sigma_r F$, or by nonradiative transitions, $T_2^S = \tau_2^{-1}$ where τ_2 is the corresponding nonradiative transition time. Free electrons are captured by ionized donors and recombine to the ground state. This process is taken into account by the coefficient T_1^S with the corresponding transition time $\tau_1 = (T_1^S N_A)^{-1}$ where N_A is the concentration of compensating acceptors. For low free electron concentrations $n << N_A$, N_A is equal to the density of ionized donors p_D. It should be emphasized that τ_1 is not the lifetime of electrons in the conduction band rather it is the mean time electrons need to return to the ground state if $n << N_A$. Typically the lifetime of electrons in the conduction band is much shorter than τ_1 [9]. Stimulated emission by free electrons is neglected due to the large density of continuum states and due to the fact that carriers

generated at higher energies relax on a picosecond time scale to the bottom of the band, thus the optical resonance condition is not met.

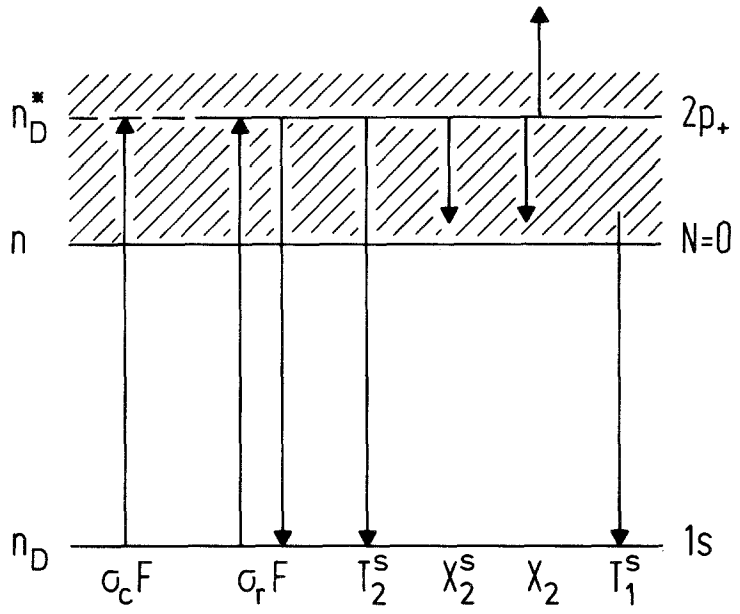

Fig. 5 — Schematic energy level diagram and generation recombination processes taken into account in the model. For details see text.

The rate equations in accordance with this model are

$$\frac{dn}{dt} = \sigma_c F\, n_D + (X_2^S + nX_2) n_{D\star} - T_1^S n p_D \tag{1}$$

$$\frac{dn_{D\star}}{dt} = \sigma_r F\,(n_{D\star} - n_D) - (X_2^S + T_2^S + nX_2) n_{D\star} \tag{2}$$

where $n, n_D, n_{D\star}$ and p_D are the concentration of electrons in the conduction band, 1s ground state electrons, $2p_+$ electrons and positive donors, respectively. From the conservation of the total donor number $N_D = n_D + n_{D\star} + p_D$ and the local neutrality condition $P_A = n_D + n_{D\star} + n$ where $P_A = N_D - N_A$ is the effective donor

concentration, the variables $n_{D^\star} = P_A - n - n_D$ and $p_D = N_A + n$ can be eliminated in the rate equations. Then one obtains in the steady state ($\frac{d}{dt} = 0$) from Eq. (2):

$$n_D = (P_A - n) \cdot \frac{\sigma_r F + T_2^S + X_2^S + nX_2}{2\sigma_r F + T_2^S + X_2^S + nX_2} \tag{3}$$

and

$$n_{D^\star} = (P_A - n) \cdot \frac{\sigma_r F}{2\sigma_r F + T_2^S + X_2^S + nX_2} \tag{4}$$

Introducing (3) and (4) into Eq.(1) leads to a relation defining the free electron concentration n:

$$g(n, F) = r(n) \tag{5}$$

where

$$g(n, F) = (P_A - n)\frac{p^\star \sigma_r F + \sigma_c F + \xi s^\star (n/P_A)(\sigma_r + \sigma_c)F + s^\star \tau_2 \sigma_r \sigma_c F^2}{1 + \xi s^\star (n/P_A) + 2s^\star \tau_2 \sigma_r F} \tag{6}$$

and

$$r(n) = n\tau_1^{-1}(1 + \frac{n}{P_A}) \tag{7}$$

are the free carrier generation and recombination rates, respectively. In Eqs.(6) and (7) we introduced the thermal ionization probability $p^* = X_2^S(X_2^S + T_2^S)^{-1}$ of the $2p_+$ state, the corresponding sticking probability $s^* = 1 - p^* = T_2^S(X_2^S + T_2^S)^{-1}$, the $2p_+$-1s nonradiative relaxation time $\tau_2 = (T_2^S)^{-1}$, the free carrier recombination time $\tau_1 = (T_1^S N_A)^{-1}$ and an impact ionization parameter $\xi = \frac{P_A X_2}{T_1^S N_A}$. The coefficient ξ is the impact ionization probability per electron in units $T_1^S N_A$ for the limiting case when all donors are ionized, i.e. $n = P_A$.

We will examine the solutions of Eq.(5) for different physical situations and compare the results to the experimental observations. For the sake of simplicity we linearize the recombination rate r(n) neglecting the n^2 term. This is justified by the fact that $n << N_A$ holds for the present experimental conditions, i.e. samples of typically 70% - 80% compensation ratio, $N_A/N_D \simeq 0.7 - 0.8$, and peak intensities lower than about 120 mW/cm^2 [8].

b) Photothermal ionization

Neglecting impact ionization, $\xi = 0$, we obtain the relation

$$(8) \qquad n(F) = P_A \tau_1 \frac{p^* \sigma_r F + \sigma_c F + s^* \tau_2 \sigma_c \sigma_r F^2}{1 + 2\tau_{eff} \sigma_r F + \tau_1 \sigma_c F + \tau_1 s^* \tau_2 \sigma_c \sigma_r F^2}$$

which has been used to evaluate high power saturation measurements performed by the UCSB Free-Electron-Laser [8]. τ_{eff} is the effective relaxation time of electrons optically excited to the $2p_+$ level [4]:

$$(9) \qquad \tau_{eff} = \frac{X_2^S + 2T_1^S N_A}{2T_1^S N_A (X_2^S + T_2^S)} = \frac{1}{2} p^* \tau_1 + s^* \tau_2.$$

Outside the impurity resonance, where $\sigma_r = 0$, the density of electrons excited into the continuum n_c is given by

$$(10) \qquad n_c(F) = P_A \tau_1 \quad \frac{\sigma_c F}{1 + \tau_1 \sigma_c F}$$

n_c must be identified with the background photosignal which was found to be linear in F up to the highest available intensities, thus $\tau_1 \sigma_c F << 1$. In this low intensity range the resonantly generated electron concentration $n_r = n - n_c$ follows from (9) and (14):

$$(11) \qquad n_r(F) = P_A \tau_1 p^* \quad \frac{\sigma_r F}{1 + F/F_S}$$

where $F_S = I_S/\hbar\omega = (2\tau_{eff} \sigma_r)^{-1}$ is the saturation photon flux density and I_S the corresponding saturation intensity [9]. This approach has been used previously to evaluate the saturation of photoconductivity [5] and it is also the basis of interpretation of absorption measurements [4,6]. Assuming the mobility to be independent of n, the dependence on F of the inverse normalized photoconductivity S is given by:

$$(12) \qquad S \propto \frac{F}{n_r} = \frac{1 + F/F_S}{P_A \tau_1 p^* \sigma_r}$$

Thus S is a linearly increasing function of F down to $F = 0$ in contrast to the experimental observations.

c) Impact ionization induced photosignal

The effect of impact ionization is most clearly demonstrated by neglecting the photoconductive background, $\sigma_c = 0$, and thus $n_c = 0$ and $n_r = n$. In Fig. 6 numerical results are presented which were obtained by solving Eq.(5) for reasonable values of τ_1/τ_2 and ξ.

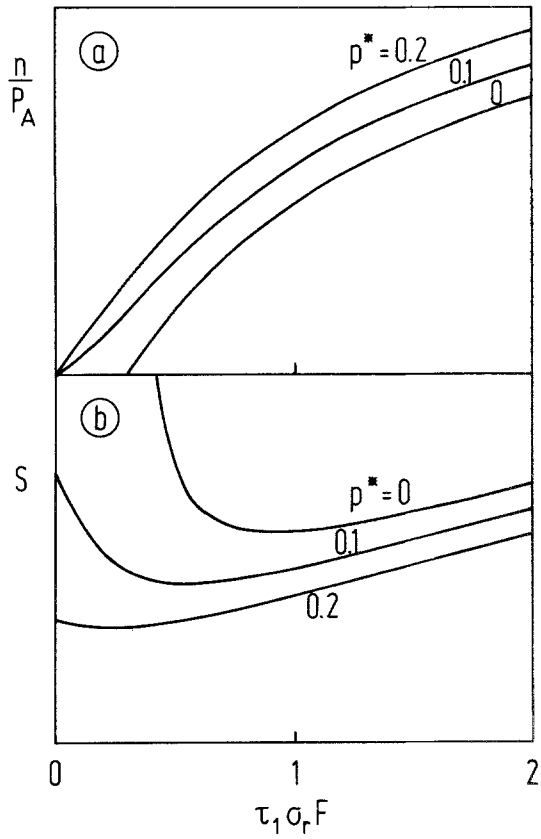

Fig. 6 — (a) Simulated photogenerated free carrier concentration n as a function of the photon flux density F. n and F are given in units of P_A and $(\tau_1 \sigma_r)^{-1}$, respectively. The kinetic parameters are: $\xi = 3$, $\tau_1/\tau_2 = 0.3$ and p^* varies from 0 to 0.2. (b) Corresponding inverse intensity normalized signal $S \propto \frac{n}{F}$ as a function of F.

The free electron density n and $S \propto \frac{F}{n}$ are plotted as functions of F for various thermal ionization probabilities p*. For vanishing p^* the optical generated electron concentration $n(F)$ shows a thresholdlike behaviour exactly like the cyclotron resonance induced photoconductivity [7]. In this case Eq.(5) has two stable solutions:

$$
\begin{aligned}
&n(F) = 0 \qquad \text{for} \quad \sigma_r F \leq (\sigma_r F)_o \\
(13) \qquad &n(F) = \eta P_A \tau_1 \frac{\sigma_r F - (\sigma_r F)_o}{1 + \tau_1 \sigma_r F} \\
&\qquad\qquad \text{for} \quad \sigma_r F > (\sigma_r F)_o
\end{aligned}
$$

where $(\sigma_r F)_o = \left((\xi - 2)\tau_2\right)^{-1}$ represents the threshold optical excitation probability which must be exceeded by $\sigma_r F$ to obtain a finite photoconductive signal. Additionally the dimensionless quantum efficiency $\eta = 1 - 2/\xi \leq 1$ has to be positive, $\eta > 0$, to get $n(F) > 0$, thus the strength of impact ionization must satisfy the condition $\xi > 2$ or $P_A X_2 > 2T_1^S N_A$. The normalized inverse signal $S \propto \frac{F}{n(F)}$ diverges at the threshold. For high intensities $n(F)$ saturates with the apparent saturation flux density $F_{SS} = (\tau_1 \sigma_r)^{-1}$. Thermal ionization of excited states smoothens the sharp onset $n(F)$ at the threshold. At low intensities $n(F)$ increases first linearly with F due to photothermal generation of electrons and proceeds superlinearly into the threshold region. The divergence of $S(F)$ is removed turning into a relative maximum at zero intensity which gets less pronounced with rising p^* and vanishes if $p^* > 1 - \frac{2\tau_{eff}}{\xi \tau_2 \beta^*}$. The apparent saturation flux density F_{SS} for large F approaches $F_S = (2\tau_{eff}\, \sigma_r)^{-1}$ corresponding to the situation of $\xi = 0$.

We now discuss the intensity dependence of the linewidth. The absorption cross section $\sigma(\omega)$ as a function of frequency is assumed to be Lorentzian shaped:

$$
(14) \qquad \sigma_r(\omega) = \sigma_{r_0} \frac{(\Delta\omega_o/2)^2}{(\omega - \omega_o)^2 + (\frac{\Delta\omega_o}{2})^2}
$$

where ω_o, $\Delta\omega_o$, and σ_{ro} are the resonance frequency, the unsaturated homogeneous linewidth and the peak absorption cross section at line center. In this case, the linewidth $\Delta\omega(F)$ as a function of photon flux density may be obtained from the relation $n = n(F)$ by

$$
(15) \qquad \left(\frac{\Delta\omega(F)}{\Delta\omega_o}\right)^2 = \frac{F}{F_{1/2}} - 1
$$

where $F_{1/2}$ is the solution of $\frac{1}{2}n(F) = n(F_{1/2})$. Numerical results of (15) are displayed in Fig. 7 for the above parameter set (s. Fig. 6) again neglecting the background photosignal, $\sigma_c = 0$. For vanishing thermal ionization probability, $p^* = 0$, a linewidth does not exist for intensities smaller than the critical threshold intensity because the line disappears as a whole. In this case one finds from (14) and (15)

$$
(16) \qquad \left(\frac{\Delta\omega(F)}{\Delta\omega_o}\right)^2 = \gamma(F)\,(1 + \tau_1 \sigma_{r_0} F)
$$

where

$$\gamma(F) = \frac{(\sigma_{r_0}F)/(\sigma_r F)_o - 1}{1 + (\tau_1 + \tau_2(\xi - 2))\sigma_{r_0}F} \tag{17}$$

for $\xi > 0$ and $\sigma_{r_0}F > (\sigma_r F)_0$. For high photon flux densities the squared linewidth approaches a linear relation $\Delta\omega(F)^2 \propto 1+F/F_{SW}$ where the apparent saturation intensity is

$$F_{SW} = (\tau_1\sigma_{r_0})^{-1} \cdot \frac{\tau_2(\xi - 2) - \tau_1}{\tau_2(\xi - 2)} = F_{SS}(1 - \tau_1(\sigma_r F)_0) \tag{18}$$

being smaller than F_{SS} which was obtained from the inverse of the intensity normalized photoconductance S. F_{SW} may even become negative, $F_{SW} < 0$, if $\tau_1(\sigma_r F)_o > 1$. For nonvanishing thermal ionization probability, $p^* > 0$, the linewidth is finite down to zero intensity and may assume a minimum for $F > 0$.

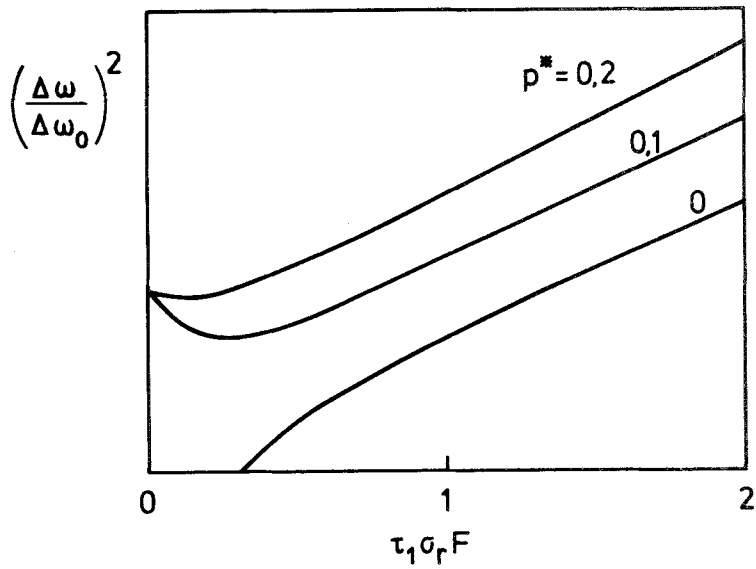

Fig. 7 — Simulated squared linewidth $\Delta\omega^2$ in units of the unsaturated squared linewidth $\Delta\omega_0^2$ as a function of photon flux density F in units of $(\tau_1\,\sigma_{r_0})^{-1}$. Parameter set as in Fig. 6.

The squared linewidths as a function of F for $p^* = 0$ and $p^* > 0$ displayed in Fig. 7 closely resemble the experimental results for low intensities at 2 K and 4.2 K, respectively, as it was shown in Fig. 4.

d) Background photoconductivity

Optical excitations of electrons directly into the conduction band yields free carriers which contribute equally well to impact ionization of the excited states like photothermally generated electrons. Thus the photoconductivity threshold is smoothened and a finite linewidth is obtained down to $F \to 0$. The superlinear onset of the photosignal still remains and gets more pronounced with increasing ratio of impact ionization to thermal ionization probability. Eq.(5) including background photoconductivity can be solved in closed form, the resulting expressions however are too clumsy for an instructive discussion.

Discussion

As shown in the above section, the observed deviation of the simple saturation behaviour expected from the photothermal process at low intensities may be qualitatively understood by assuming impact ionization of the excited $2p_+$-state. This effect occurs for bias voltages well below the impact ionization breakdown of the non-irradiated sample because the binding energy of the excited state is much smaller than that of the ground state which is predominantly populated at low temperatures. In cases when the $2p_+$-level is in the $N = 0$ Landau continuum an angular momentum relaxing electron impact is sufficient to ionize the excited donors. Even for zero bias voltage excited state impact ionization is expected to occur due to the nonthermal distribution of optically generated electrons.

The experimental results were simulated by numerical solution of Eq.(5). Best fits were obtained using the parameters summarized in Tab. 1 and 2. In spite of the large number of parameters involved

Table 1. — Unsaturated linewidth $\Delta\omega_o$, peak resonant absorption cross section σ_{ro}, thermal ionization probability p^*, free carrier recombination time τ_1, $2p_+ \to 1s$ transition time τ_2 and effective recombination time of $2p_+$ electrons τ_{eff} for 4.2 K and 2 K.

T(K)	$\Delta\omega_o$ (cm^{-1})	σ_{ro} (cm^2)	p^*	τ_1 (ns)	τ_2 (ns)	τ_{eff} (ns)
4.2	0.63	$4.32 \cdot 10^{-12}$	0.28	29	12	12.4
2	0.49	$5.55 \cdot 10^{-12}$	$4.9 \cdot 10^{-3}$	10	50	49.8

in the rate equation model a well defined set of parameters could be obtained by fitting both the peak signal and the linewidth as functions of intensity. The numerical results are displayed in Figs. 2,3 and 4 as full lines. Excellent agreement between the measurements and the calculated curves are obtained for the peak photosignal shown in Figs. 2 and 3. The low intensity anomaly of the power broadening plotted in Fig. 4 is reasonably well reproduced by the calculations. For higher intensities however, in particular at 4.2 K, the line broadens stronger with increasing intensity than predicted by our model. We have no stringent explanation for this phenomena. It might be that heating of the sample yields this additional broadening as it has been observed for optical transitions between excited states at temperatures above liquid helium temperature [14]. As it is not obvious how to extrapolate the measured linewidth to zero intensity (s. Fig. 4), the unsaturated linewidth $\Delta\omega_o$ had to be included into the fitting procedure. The peak resonant cross section σ_{ro} was then calculated from the oscillator strength obtained from the theoretical work of Forster et al. [15]. Finally the photoionization cross section σ_c was estimated after [16] to be $\sigma_c = 10^{-2}\,\sigma_{ro}$. The remaining kinetic parameters were determined by fitting. Table 1 summarizes $\Delta\omega_o$, σ_{ro}, and parameters due to thermal processes p^*, τ_1, τ_2 determined for 4.2 K and 2 K . This parameter set was found to be practically independent of the bias voltage as long as the sample was biased well below the threshold of impact ionization instability. In Tab. 2 the impact ionization parameter X_2 and $X_2 P_A / X_2^S$ is listed for both temperatures and both bias fields of the present investigation. $X_2 P_A / X_2^S$ denotes the ratio of the excited state impact ionization rate in the limit of fully ionized donors to the rate of thermal ionization.

Table 2. — Impact ionization parameter for two different bias fields E at 4.2 K and 2 K. X is the impact ionization probability per electron; XP_A/X_2^S is the ratio of impact ionization rate to thermal ionization rate in the limiting case of fully ionized donors.

T(K)	E (V/cm)	X (cm^3/s)	XP_A/X_2^S
4.2	2	$3.2 \cdot 10^{-7}$	1.22
	3.2	$5.3 \cdot 10^{-7}$	2.0
2	1	$4.3 \cdot 10^{-6}$	$5.64 \cdot 10^3$
	5.2	$5.2 \cdot 10^{-6}$	$6.74 \cdot 10^3$

At 4.2 K thermal ionization of the excited state dominates the strength of the photoconductive signal. The impact ionization parameter $X_2 P_A$, which increases slightly with rising bias electric field, is of the same order of magnitude as the thermal ionization parameter X_2^S. However, as $n << P_A$ even for large intensities [8], the actual impact ionization rate is much smaller than the thermal ionization rate. The effective recombination time τ_{eff} is practically the same as it may be obtained neglecting the effect of excited state impact ionization and evaluating the measurements by the simple relation $S \propto 1 + I/I_s$ as it has been done in previous investigations. In spite of the marginal effect of impact ionization on the photoconductive signal strength, the power broadening of the linewidth is strongly affected. The variation of $\Delta\omega$ at low intensities cannot be described without taking into account impact ionization of the $2p_+$ state.

Reducing the temperature to 2 K lowers the thermal ionization probability by two orders of magnitude and raises the impact ionization parameter by three orders of magnitude. At this temperature the photoconductive signal is mainly due to impact ionization of the $2p_+$-state. The recombination time of free carriers τ_1 decreases from 29 ns at 4.2 K to 10 ns at 2 K indicating the increase of the thermal capture cross section. The $2p_+$-1s transition time rises from 12 ns to 50 ns. Thus the majority of optically excited electrons remain stuck on the donator and τ_{eff} is practically equal to τ_2. In this case evaluating the high power data according $S \propto 1 + I/I_s$ yields definitely wrong values of τ_{eff}.

Conclusion

In summary, we have investigated the saturation behaviour of the resonant magneto-photoconductivity due to 1s-$2p_+$ transitions of shallow donors in high purity n-GaAs epitaxial layers. Special emphasis was put on low intensity data where characteristic anomalies were observed being present both in the intensity dependence of the peak photosignal and in the power broadening of the linewidth. The observed effects could be attributed to impact ionization of the optically excited $2p_+$ state in addition to thermal ionization. Our analysis clarifies already previously observed discrepancies between

the intensity dependence of the photosignal and that of linewidth which have not yet been explained [5].

At 4.2 K the impact ionization rate of the $2p_+$ state was found to be much smaller than the thermal ionization rate. Thus excited state impact ionization has only a little effect on the signal strength. The evaluation of the electron kinetics in earlier work based on the power dependence of the photoconductive signal or the absorption coefficient seems to yield correct quantitative results. Power broadening of the linewidth however, which, unlike the signal strength, has been disregarded in almost all previous publications, is non-negligibly affected by excited state impact ionization in particular at low power levels. The linewidth as a function of intensity cannot be described, even at 4.2 K, without taking into account impact ionization.

Reducing the temperature to 2 K changes the electron kinetics drastically. The impact ionization rate is now about three orders of magnitude larger than the thermal ionization rate. Excited state impact ionization almost exclusively causes the resonant photoconductive signal and controls the signal strength and the linewidth as functions of intensity.

Acknowledgement

Financial support by the Deutsche Forschungsgemeinschaft is gratefully acknowledged.

References

[1] T. Murotani and Y. Nisida, J. Phys. Soc. Jpn. **32**, 986 (1972).
[2] E. Gornik, T.K. Chang, T.J. Bridges, V.T. Nguyen, I.D. McGee, and W. Müller, Phys. Rev. Letters **40**, 1151 (1978).
[3] K. Muro, N. Yutani, and Sh. Narita, J. Phys. Soc. Jpn. **49**, 593 (1980).
[4] C.R. Pidgeon, A. Vass, G.R. Allan, W. Prettl, and L.A. Eaves, Phys. Rev. Letters **50**, 1309 (1983).
[5] W. Prettl, A. Vass, G.R. Allan, and C.R. Pidgeon, Int. J. Infrared and Millimeter Waves **4**, 561 (1983).
[6] G.R. Allan, A. Black, C.R. Pidgeon, E. Gornik, W. Seidenbusch, and P. Colter, Phys. Rev. **B 31**, 3560 (1985).

[7] M. Weispfenning, I. Hoeser, W. Böhm, and W. Prettl, Phys. Rev. Letters **55**, 754 (1985).

[8] J. Kaminski, J. Spector, W. Prettl, and M. Weispfenning, Appl. Phys. Letters **52**, 233 (1988).

[9] J. Kaminski, J. Spector, W. Prettl, and M. Weispfenning, Int. J. Infrared and Millimeter Waves, vol. 9, no.9, Sept. 1988

[10] Sh.M. Kogan and B.I. Sedunov, Sov. Phys.-Solid State **8**, 1898 (1967).

[11] R.H. Pantell and H.E. Puthoff, *Fundamentals of Quantum Electronics*, New York: Wiley, 1969.

[12] H.J.A. Bluyssen, I.C. Maan, T.B. Tan, and P. Wyder, Phys. Rev. **B 22**, 749 (1980).

[13] H.P.Wagner and W. Prettl, Solid State Commun. **66**, 367 (1988).

[14] I. Golka, J. Trylski, M.S. Skolnick, R.A. Stradling, and Y. Conder, Solid State Commun. **22**, 623 (1977).

[15] H. Forster, W. Strupat, W. Rösner, G. Wunner, H. Ruder and H. Herold, J. Phys. **B 17**, 1301 (1984).

[16] H. Hasegawa and R.E. Howard, J. Phys. Chem. Solids **21**, 179 (1961).